The Astronomical Journal, 139:1844–1856, 2010 May doi:10.1088/0004-6256/139/5/1844

THE MASS OF HD 38529c FROM *HUBBLE SPACE TELESCOPE* ASTROMETRY AND HIGH-PRECISION RADIAL VELOCITIES*

G. Fritz Benedict[1], Barbara E. McArthur[1], Jacob L. Bean[2,8], Rory Barnes[3], Thomas E. Harrison[4], Artie Hatzes[5], Eder Martioli[6], and Edmund P. Nelan[7]

[1] McDonald Observatory, University of Texas, Austin, TX 78712, USA
[2] Institut für Astrophysik, Georg-August-Universität Göttingen, Friedrich-Hund-Platz 1, 37077 Göttingen, Germany
[3] Department of Astronomy, University of Washington, Seattle, WA 98195, USA
[4] Astronomy Department, New Mexico State University, Las Cruces, NM 88003, USA
[5] Thuringer Landessternwarte, Tautenburg, D-07778, Germany
[6] Instituto Nacional de Pesquisas Espaciais, S. J. dos Campos, SP, Brazil
[7] Space Telescope Science Institute, 3700 San Martin Drive, Baltimore, MD 21218, USA

Received 2010 January 26; accepted 2010 February 27; published 2010 April 1

ABSTRACT

Hubble Space Telescope Fine Guidance Sensor astrometric observations of the G4 IV star HD 38529 are combined with the results of the analysis of extensive ground-based radial velocity (RV) data to determine the mass of the outermost of two previously known companions. Our new RVs obtained with the Hobby–Eberly Telescope and velocities from the Carnegie–California group now span over 11 yr. With these data we obtain improved RV orbital elements for both the inner companion, HD 38529b, and the outer companion, HD 38529c. We identify a rotational period of HD 38529 ($P_{\rm rot} = 31.65 \pm 0.^{\rm d}17$) with Fine Guidance Sensor photometry. The inferred star spot fraction is consistent with the remaining scatter in velocities being caused by spot-related stellar activity. We then model the combined astrometric and RV measurements to obtain the parallax, proper motion, perturbation period, perturbation inclination, and perturbation size due to HD 38529c. For HD 38529c we find $P = 2136.1 \pm 0.3$ d, perturbation semimajor axis $\alpha = 1.05 \pm 0.06$ mas, and inclination $i = 48.^{\circ}3 \pm 3.^{\circ}7$. Assuming a primary mass $M_* = 1.48\,M_\odot$, we obtain a companion mass $M_c = 17.6^{+1.5}_{-1.2}\,M_{\rm Jup}$, 3σ above a 13 $M_{\rm Jup}$ deuterium burning, brown dwarf lower limit. Dynamical simulations incorporating this accurate mass for HD 38529c indicate that a near-Saturn mass planet could exist between the two known companions. We find weak evidence of an additional low amplitude signal that can be modeled as a planetary-mass ($\sim$0.17 $M_{\rm Jup}$) companion at $P \sim 194$ days. Including this component in our modeling lowers the error of the mass determined for HD 38529c. Additional observations (RVs and/or *Gaia* astrometry) are required to validate an interpretation of HD 38529d as a planetary-mass companion. If confirmed, the resulting HD 38529 planetary system may be an example of a "Packed Planetary System."

Key words: astrometry – brown dwarfs – stars: distances – stars: individual (HD 38529) – stars: late-type – techniques: interferometric – techniques: radial velocities

Online-only material: color figures

1. INTRODUCTION

HD 38529 (= HIP 27253 = HR 1988 = PLX 1320) hosts two known companions discovered by high-precision radial velocity (RV) monitoring (Fischer et al. 2001, 2003; Wright et al. 2009). Previously published periods were $P_b = 14.31$ days and $P_c = 2146$ days with minimum masses $M_b \sin i = 0.85\,M_{\rm Jup}$ and $M_c \sin i = 13.1\,M_{\rm Jup}$, the latter right above the currently accepted brown dwarf mass limit. A predicted minimum perturbation for the outermost companion, HD 38529c, $\alpha_c = 0.8$ mas, motivated us to obtain millisecond of arc per-observation precision astrometry with *Hubble Space Telescope* (*HST*) with which to determine its true mass (not the minimum mass, $M_c \sin i$). These astrometric data now span 3.25 yr.

In the early phases of our project, Reffert & Quirrenbach (2006) derived an estimate of the mass of HD 38529c from *Hipparcos*, obtaining $M_c = 38^{+36}_{-19}\,M_{\rm Jup}$, well within the brown dwarf "desert." Recent comparisons of Fine Guidance Sensor (FGS) astrometry with *Hipparcos*, e.g., van Leeuwen et al. (2007), suggest that we should obtain a more precise and accurate mass for HD 38529c. Our mass is derived from combined astrometric and RV data, continuing a series presenting accurate masses of planetary, brown dwarf, and non-planetary companions to nearby stars. Previous results include the mass of Gl 876b (Benedict et al. 2002a), of ρ^1 Cancri d (McArthur et al. 2004), ϵ Eri b (Benedict et al. 2006), HD 33636B (Bean et al. 2007), and HD 136118 b (Martioli et al. 2010).

HD 38529 is a metal-rich G4 IV star at a distance of about 40 pc. The star lies in the "Hertzsprung Gap" (Murray & Chaboyer 2002), a region typically traversed very quickly as a star evolves from dwarf to giant. Baines et al. (2008b) have measured a radius. HD 38529 also has a small IR excess found by Moro-Martín et al. (2007) with *Spitzer* and interpreted as a Kuiper Belt at 20–50 AU from the primary. Stellar parameters are summarized in Table 1.

In Section 2, we model RV data from four sources, obtaining orbital parameters for both HD 38529b and HD 38529c. We also discuss and identify RV noise sources. In Section 3, we present the results of our combined astrometry/RV modeling,

* Based on observations made with the NASA/ESA *Hubble Space Telescope*, obtained at the Space Telescope Science Institute, which is operated by the Association of Universities for Research in Astronomy, Inc., under NASA contract NAS5-26555. Based on observations obtained with the Hobby–Eberly Telescope, which is a joint project of the University of Texas at Austin, the Pennsylvania State University, Stanford University, Ludwig-Maximilians-Universität München, and Georg-August-Universität Göttingen.

[8] Marie Curie International Incoming Fellow.

Table 1
HD 38529 Stellar Parameters

Parameter	Value	Source
SpT	G4 IV	1, 9
$T_{\rm eff}$	5697 K	2
log g	3.94 ± 0.1	2
[Fe/H]	0.27 ± 0.05	2
Age	3.28 ± 0.3 *By*	2
Mass	1.48 ± 0.05 $M_\odot$	2
Distance	40.0 ± 0.5 *pc*	3
R	2.44 ± 0.22 $R_\odot$	4
$v \sin i$	3.5 ± 0.5 km s^{-1}	5
V	5.90 ± 0.03	6
K	4.255 ± 0.03	7
$V-K$	1.65 ± 0.04	
$i-z$	0.06	8
$g-r$	0.55	8
$r-i$	0.15	8

References. (1) Fischer et al. 2001; (2) Takeda 2007 or Takeda et al. 2007; (3) parallax from Table 10; (4) Baines et al. 2008b; (5) Valenti & Fischer 2005; (6) SIMBAD; (7) 2MASS; (8) Ofek 2008; (9) Murray & Chaboyer 2002.

concentrating on HD 38529c. We briefly discuss the quality of our astrometric results as determined by residuals, and derive an absolute parallax and relative proper motion for HD 38529, those nuisance parameters that must be removed to determine the perturbation parameters for the perturbation due to component c. Simultaneously we derive the astrometric orbital parameters. These, combined with an estimate of the mass of HD 38529, provide a mass for HD 38529c. Section 4 contains the results of searches for additional components, limiting the possible masses and periods of such companions. In Section 5, we discuss possible identification of an RV signal that remained after modeling components b and c. We discuss our results and summarize our conclusions in Section 6.

2. RADIAL VELOCITIES

2.1. RV Orbits

We first model RV data, a significant fraction of which comes from the Hobby–Eberly Telescope (HET). Measurements from the California–Carnegie exoplanet research group (Wright et al. 2009) and a few from the McDonald Harlan J. Smith telescope (Wittenmyer et al. 2009) were also included. The California–Carnegie data were particularly valuable, increasing the time span from 4 to over 11 yr. Our astrometry covers only ∼70% of the orbit of HD 38529c, and in the absence of a multi-period span of RVs, would not be sufficient to establish accurate perturbation elements, particularly period, eccentricity, and periastron passage. All RV sources are listed in Table 2, along with the rms of the residuals to the combined orbital fits described below. The errors for all published RV and our new HET RV have been modified by adding in quadrature the expected RV jitter from stellar activity determined in Section 2.2.

All the RVs were obtained using I_2 cell techniques. The HET data were obtained with the HET High-resolution Spectrograph, described in Tull (1998) and processed with the I_2 pipeline described in Bean et al. (2007), utilizing robust estimation to combine the all velocities from the individual chunks. Typically three HET observations are secured within 10–15 minutes. These are combined using robust estimation to form normal points for each night. The HET normal points and associated errors are listed in Table 3.

Table 2
The RV Data Sets

Data Set	Coverage	Nobs	rms (m s^{-1})	
			3C[a]	2C[b]
Lick	1998.79−2008.22	109	10.34	10.74
HJS	1995.72−1996.78	7	7.24	7.56
Keck	1996.92−2008.07	55	7.39	7.90
HET	2004.92−2008.98	313[c]	5.75	5.92
	Total	484		

Notes.
[a] Solution including components b, c, and d.
[b] Solution including components b, c only.
[c] Reduced to 102 normal points.

Combining RV observations from different sources is possible in the modeling environment we use. GaussFit (Jefferys et al. 1988) has the capability to simultaneously solve for many separate velocity offsets (because velocities from different sources are relative, having differing zero points), along with the other orbital parameters. Relative offsets (γ) and associated errors are listed in Table 11.

Orbital parameters derived from a combination of HET, HJS, Lick, and Keck RVs and *HST* astrometry will be provided in Section 3.5. Figure 1 shows the entire span of data along with the best-fit multiple-Keplerian orbit. We note that there is sufficient bowing in the residuals to justify continued low-cadence RV monitoring, particularly given the prediction of Moro-Martín et al. (2007) of dynamical stability for planets with periods as short as ∼70 yr. Subtracting in turn the signature of first one, then the other known companion from the original velocity data we obtain the component b and c RV orbits shown in Figure 2, each phased to the relevant periods. Re-iterating, all RV fits were modeled simultaneously with the astrometry.

Compared to the typical perturbation RV curve (e.g., Hatzes et al. 2005; McArthur et al. 2004; Cochran et al. 2004), our original orbits for components b and c exhibited significant scatter, much due to the identified stellar noise source discussed in Section 2.2 below. Periodogram analysis of RV residuals to simultaneous fits of components b and c indicated a significant peak with a period near 197 days. The existence of the signal is fairly secure. A bootstrap analysis carried out by randomly shuffling the RV residual values 200,000 times (keeping the times fixed), and determining if the random data periodogram had peaks higher than the real data periodogram in the frequency range $0 < \nu < 0.02$ day^{-1}, yielded a false alarm probability, FAP $= 5 \times 10^{-4}$. This motivated the addition of a third Keplerian component, resulting in the fit shown in the bottom panel of Figure 2. Even though the amplitude of this signal is about that expected from stellar noise, including this component (five additional parameters) in the combined modeling improved both the reduced χ^2, and the rms scatter as shown in Table 2. Identification of the cause of the signal will be discussed further in Section 5.

2.2. Stellar Rotation and the RV Noise Level

There are a number of sources of RV noise intrinsic to HD 38529: pulsations and velocity perturbations introduced by star spots and/or plages. The velocity effects caused by the latter two are modulated by stellar rotation. Valenti & Fischer (2005)

Table 3
HET RV Data

JD-2450000	RV (m s^{-1})	± Error
3341.779899	−105.27	7.77
3341.898484	−118.43	7.25
3355.845730	−102.05	7.34
3357.859630	−105.27	7.48
3358.724097	−87.82	7.11
3359.729188	−82.07	8.70
3360.849520	−65.85	7.80
3365.817387	1.45	7.73
3367.812640	−20.41	9.48
3369.701315	−90.14	8.57
3371.684761	−107.83	8.90
3377.785833	−20.51	8.92
3379.675805	−3.53	6.78
3389.755622	−50.16	7.68
3390.763879	−35.52	7.46
3391.757235	−19.07	8.15
3392.750785	−5.45	7.11
3395.738803	2.78	6.97
3414.693834	−103.63	10.96
3416.683636	−74.10	8.61
3665.892690	64.01	4.74
3675.986919	6.80	5.07
3676.846929	21.68	5.48
3678.862452	42.80	5.63
3681.843596	51.51	5.06
3685.835951	−63.04	25.10
3685.837515	−57.70	5.16
3691.933851	27.17	5.07
3692.834053	39.74	5.00
3694.820769	63.79	5.48
3695.817331	61.75	5.81
3696.807526	47.54	4.91
3697.813712	8.53	5.32
3700.809061	−38.81	5.48
3708.894418	64.36	6.38
3709.886951	60.71	5.85
3711.767580	20.98	5.68
3712.875847	−26.85	7.10
3724.839770	60.73	6.27
3730.717661	−28.39	7.05
3731.708724	−18.87	6.85
3733.706335	16.30	6.90
3735.713861	48.56	6.86
3739.692156	48.28	6.40
3742.684910	−46.27	5.94
3751.775752	73.88	6.84
3752.761925	74.25	6.79
3753.773028	64.34	7.73
3754.760139	35.42	6.79
3755.751319	−9.88	6.38
3757.639021	−39.51	6.53
3758.754961	−29.76	6.22
3764.745400	62.37	6.78
3989.998171	88.56	5.09
4020.924198	141.62	5.36
4021.921835	158.20	5.52
4022.926094	164.55	8.27
4028.903039	75.06	5.75
4031.882076	104.25	5.64
4031.997118	111.67	5.86
4035.887008	164.27	6.09
4037.876174	185.49	5.35
4039.869089	180.04	5.69
4040.971815	145.86	5.30
4043.860701	95.53	5.43
4048.842947	150.59	5.30

Table 3
(Continued)

JD-2450000	RV (m s^{-1})	± Error
4048.939538	149.37	7.22
4051.843854	187.96	5.64
4052.839025	197.86	5.30
4053.847354	193.90	6.22
4054.832617	170.75	5.14
4056.922854	86.05	5.72
4060.915198	100.89	5.56
4061.912707	128.08	5.65
4062.807028	136.95	5.26
4063.809422	157.36	4.87
4071.890292	91.98	5.58
4072.774474	89.84	6.22
4073.892958	100.30	5.66
4075.757176	129.10	5.57
4105.804643	175.94	7.08
4109.801302	221.86	6.78
4110.690995	223.57	6.45
4121.646747	210.00	7.33
4128.729702	122.64	7.65
4132.725529	163.95	10.45
4133.718796	165.86	6.92
4163.637004	202.53	6.48
4373.962556	210.00	8.54
4377.933380	277.65	4.60
4398.878305	269.02	5.90
4419.843012	243.10	5.81
4424.821940	314.81	4.42
4425.816251	307.27	6.65
4475.769793	190.40	7.04
4487.651953	153.73	6.93
4503.606266	151.66	7.95
4520.665744	175.50	6.58
4726.967268	61.40	8.31
4729.974635	−45.60	6.43
4808.884683	8.79	7.32
4822.725625	18.40	6.72

measure a rotation of HD 38529, $V_{rot} \sin i = 3.5 \pm 0.5$ km s^{-1}. HD 38529 is subgiant star, evolving toward the giant branch of the Hertszprung–Russell diagram, and is expected to have a higher level of pulsational activity than a main sequence star (Hatzes & Zechmeister 2008). The pulsational amplitude can be estimated using the scaling relationship of Kjeldsen & Bedding (1995) $V_{amp} = (L/L_{\odot})/(M/M_{\odot}) \times 0.234$ m s^{-1}. The luminosity and mass of HD 38529 yield a pulsational amplitude of ∼1 m s^{-1}, so this alone cannot account for the excess RV scatter.

Several relationships between the amplitude of RV noise and the fraction of star spot coverage have been developed. Saar & Donahue (1997) obtain $A_{RV} = 6.5 \times v \sin i \times f^{0.9}$, where f is the spot filling factor in percent. Hatzes (2002) obtained $A_{RV} = (8.6v \sin i - 1.6) \times f^{0.9}$. We can estimate the spot filling factor from FGS photometry of HD 38529. The FGS has been shown to be a photometer precise at the 2 mmag level (Benedict et al. 1998). We flat-fielded the HD 38529 FGS photometry, using an average of the counts from the astrometric reference stars listed in Table 5, and plotted it against time. Clearly not constant at a level ten times our internal precision, a Lomb–Scargle periodogram showed a significant period at $P =$ 31.6 days (FAP $= 4.3 \times 10^{-4}$). A sine wave fit to the photometry yielded $P = 31.65 \pm 0.^{d}17$ with an amplitude $= 1.5 \pm 0.2$ mmag. Figure 3 is a plot of these photometric data phased to that period.

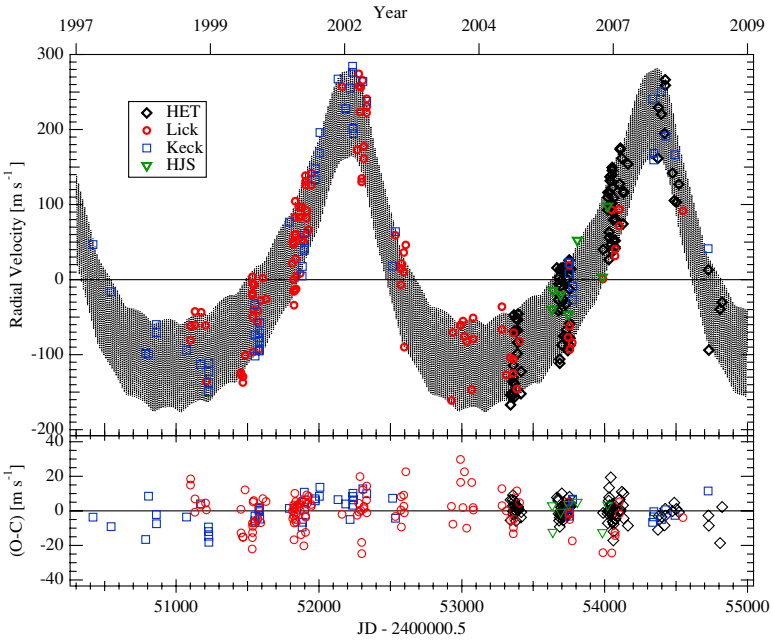

Figure 1. RV measurements of HD 38529 from sources as indicated in the legend (and identified in Table 2). The line is the velocity predicted from the orbital parameters (Table 11) derived in the combined solution. Residuals (RV observed minus RV calculated from the orbit) are plotted at bottom.
(A color version of this figure is available in the online journal.)

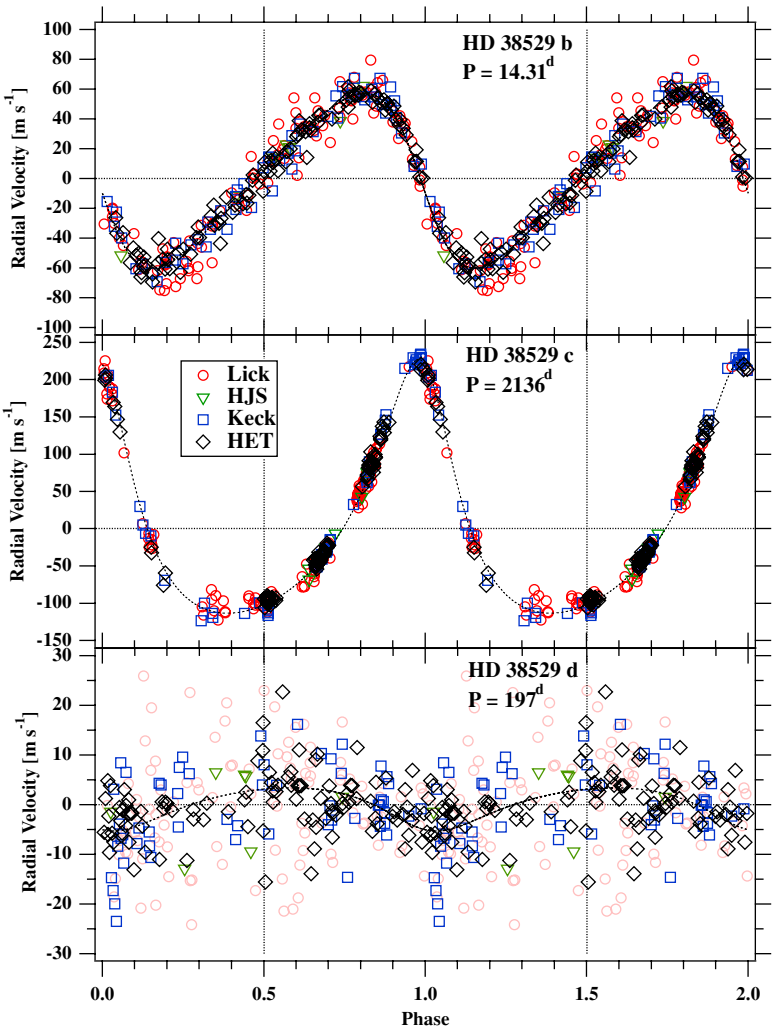

Figure 2. RV measurements of HD 38529 from sources as indicated in the legend (and identified in Table 2) phased to the orbital periods determined from a combined solution including astrometry and RV (Section 3.5). The dashed line is the velocity predicted from the orbital parameters (Table 11) derived in the combined solution.
(A color version of this figure is available in the online journal.)

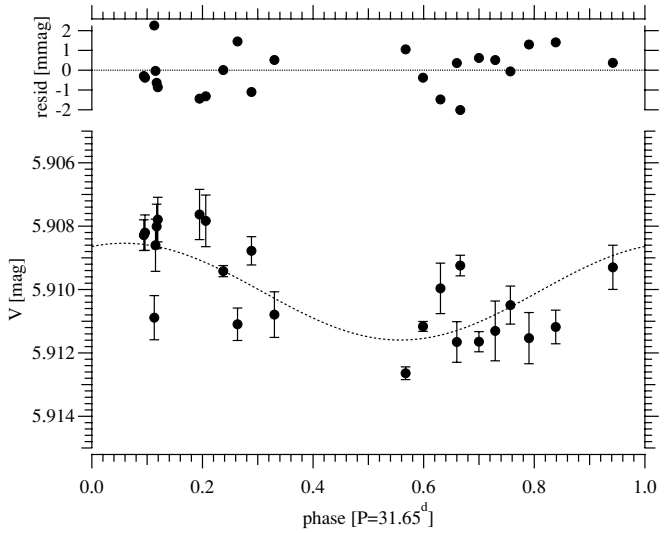

Figure 3. FGS photometry of HD 38529 phased to a period, $P = 31.65$ days. HD 38529 intensities were flat-fielded with average counts from all astrometric reference stars observed during each observation set. Normal points are formed from the five observations of HD 38529 secured within each set. The zero-point is chosen so that the average V magnitude matches the SIMBAD value. The amplitude of the photometric variation is 0.15%. A periodogram of the flat-field values shows no significant signals in the range $10 < P < 70$ days.

The Valenti & Fischer (2005) $V_{\rm rot}$ sin $i = 3.5$ km s^{-1} and a stellar radius from Baines et al. (2008b), $R = 2.44 \pm 0.22\,R_{\odot}$, would predict a minimum $P_{\rm rot} = 32 \pm 5$ days. Interpreting the modulation period of 31.6 days as the stellar rotation period, we ascribe the photometric variation (0.15%) to rotational modulation of star spots. The photometric amplitude suggests an RV noise level of 4–5 m s^{-1}. Taking the HET velocity rms as closer to the true RV variation, we identify the remaining RV scatter as a combination of the three effects identified.

3. *HST* ASTROMETRY

We used *HST* FGS 1r (FGS1r) to carry out our space-based astrometric observations. Nelan (2007) provides a detailed overview of FGS1r as a science instrument. Benedict et al. (2002b, 2006) describe the FGS3 instrument's astrometric capabilities along with the data acquisition and reduction strategies used in the present study. We use FGS1r for the present study because it provides superior fringes from which to obtain target and reference star positions (McArthur et al. 2002).

HD 38529 is shown in Figure 4 along with the astrometric reference stars used in this study. Table 4 presents a log of *HST* FGS observations. Note the bunching of the observation sets, each "bunch" with a time span less than a few days. Each set is tagged with the time of the first observation within each set. The field was observed at a very limited range of spacecraft roll values. As shown in Figure 5, HD 38529 had to be placed in different locations within the FGS1r FOV to accommodate the distribution of astrometric reference stars and to ensure availability of guide stars required by the other two FGS units. Additionally, all observation sets suffered from observation timing constraints imposed by two-gyro guiding.[9] Note that due to the extreme bunching of the epochs, we acquired effectively only five astrometric epochs. Also, we note that the last group of observation sets were a "bonus." In 2008 November, the only science instrument operating on *HST* was FGS1r. Consequently,

[9] *HST* has a full compliment of six rate gyros, two per axis, that provide coarse pointing control. By the time these observations were in progress, three of the gyros had failed. *HST* can point with only two. To "bank" a gyro in anticipation of a future failure, NASA decided to go to two gyro pointing as a standard operating procedure.

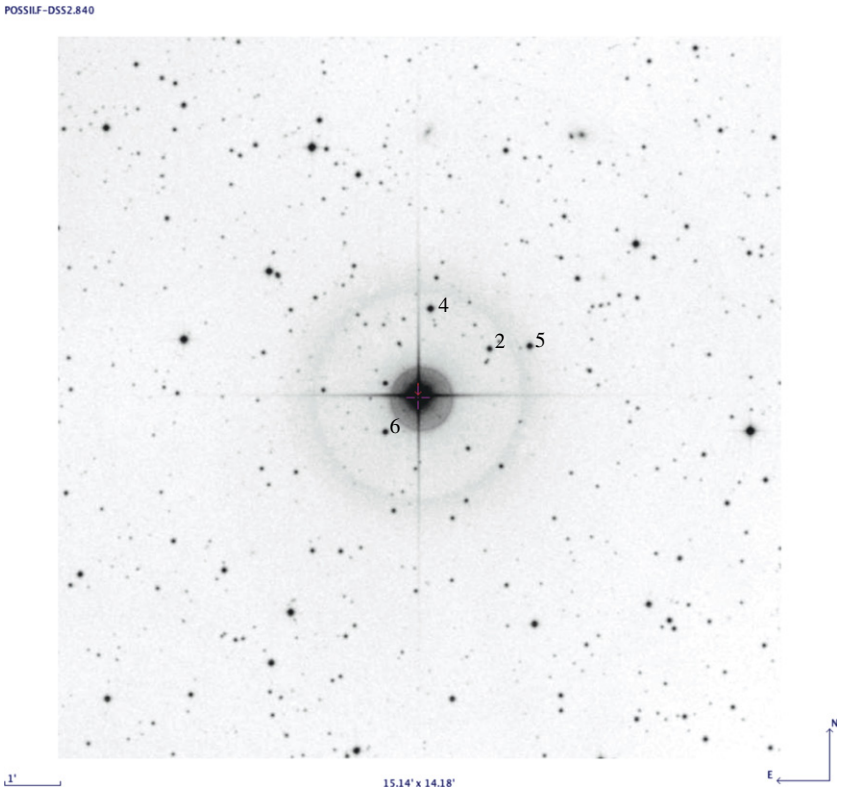

Figure 4. Positions of HD 38529 (center) and the astrometric reference stars identified in Table 5.

Table 4
Log of HD 38529 FGS Observations

Epoch	MJD[a]	Year	Roll (°)[b]
1	53597.05445	2005.619588	285.709
2	53599.2528	2005.625607	284.644
3	53600.11884	2005.627978	284.236
4	53601.18477	2005.630896	283.74
5	53605.98201	2005.64403	281.607
6	53613.97829	2005.665923	280.001
7	53689.06154	2005.87149	244.998
8	53690.05794	2005.874217	244.998
9	53691.05421	2005.876945	244.998
10	53692.18891	2005.880052	244.998
11	53693.25725	2005.882977	244.998
12	53697.65138	2005.895007	244.998
13	53964.25536	2006.624929	284.764
14	53965.05198	2006.62711	284.386
15	54057.37329	2006.879872	244.998
16	54058.37467	2006.882614	244.998
17	54061.30276	2006.89063	244.998
18	54781.68145	2008.86292	250.063
19	54781.74804	2008.863102	250.063
20	54782.28072	2008.864561	250.063
21	54782.34731	2008.864743	250.063
22	54782.41389	2008.864925	250.063
23	54782.48048	2008.865107	250.063

Notes.
[a] MJD = JD − 2400000.5.
[b] Spacecraft roll as defined in Chapter 2, FGS Instrument Handbook (Nelan 2007).

Table 5
Astrometric Reference Stars

ID	R.A.[a] (2000.0)	Decl.[a]	V[b]
2	86.624482	1.182386	14.12
4	86.642054	1.194295	13.05
5	86.612529	1.183187	13.87
6	86.655567	1.157715	14.34

Notes.
[a] Positions from 2MASS.
[b] Magnitudes from NMSU.

Table 6
V and Near-IR Photometry

ID	V	K	$(J-H)$	$(J-K)$	$(V-K)$
1	5.9 ± 0.03	4.255 ± 0.036	0.58 ± 0.24	0.73 ± 0.23	1.65 ± 0.05
2	14.12 0.03	11.88 0.021	0.44 0.03	0.49 0.03	2.24 0.04
4	13.05 0.03	11.239 0.024	0.29 0.04	0.35 0.04	1.81 0.04
5	13.87 0.03	10.303 0.023	0.75 0.03	0.90 0.03	3.57 0.04
6	14.34 0.03	10.567 0.021	0.70 0.03	0.93 0.03	3.77 0.04

we were able to acquire additional observation sets for a few of our prime science targets, including HD 38529. These recent data significantly lengthened the time span of our observations, hence, increased the precision with which the parallax and proper motion could be removed to determine the perturbation orbit of HD 38529. Once combined with an estimate of the mass of HD 38529, the perturbation size will provide the mass of the companion, HD 38529c.

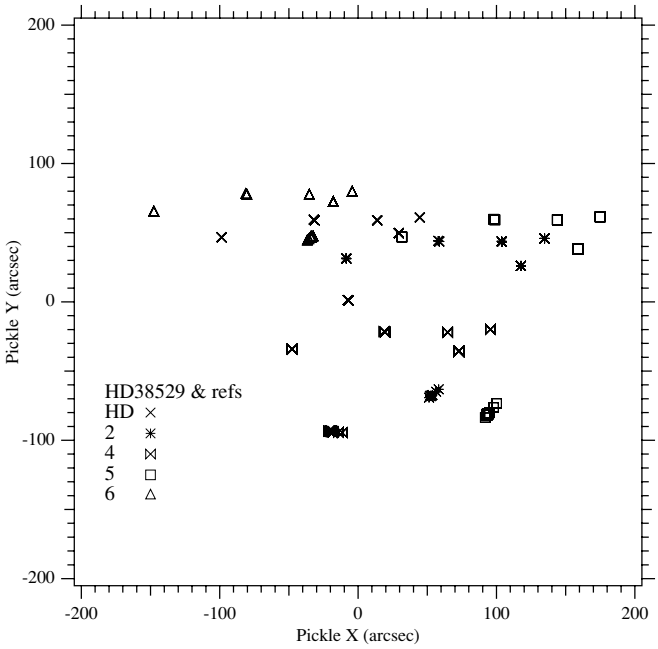

Figure 5. Positions of HD 38529 and astrometric reference stars in FGS1r "pickle" coordinates. Due to two-gyro guiding constraints and guide star availability it was not possible to keep HD 38529 in the pickle center at each epoch.

3.1. HD 38529 Astrometric Reference Frame

The astrometric reference frame for HD 38529 consists of four stars. Any prior knowledge concerning these four stars eventually enters our modeling as observations with error and yields the most accurate parallax and proper motion for the prime target, HD 38529. These periodic and non-periodic motions must be removed as accurately and precisely as possible to obtain the perturbation inclination and size caused by HD 38529c. Of particular value are independently measured proper motions. This particular prior knowledge comes from the UCAC3 catalog (Zacharias et al. 2010). Figure 5 shows the distribution in FGS1r pickle coordinates of the 23 sets of four reference star measurements for the HD 38529 field. At each epoch we measured each reference stars two to four times, and HD 38529 five times.

3.2. Absolute Parallaxes for the Reference Stars

Because the parallax determined for HD 38529 is measured with respect to reference frame stars which have their own parallaxes, we must either apply a statistically derived correction from relative to absolute parallax (van Altena et al. 1995, Yale Parallax Catalog, YPC95), adopt an independently derived parallax (e.g., *Hipparcos*), or estimate the absolute parallaxes of the reference frame stars. In principle, the colors, spectral type, and luminosity class of a star can be used to estimate the absolute magnitude, M_V, and V-band absorption, A_V. The absolute parallax for each reference star is then simply,

$$\pi_{\rm abs} = 10^{-(V-M_V+5-A_V)/5}. \quad (1)$$

3.2.1. Reference Star Photometry and Spectroscopy

Our band passes for reference star photometry include *BVRI* photometry of the reference stars from the NMSU 1 m telescope located at Apache Point Observatory and *JHK* (from the Two

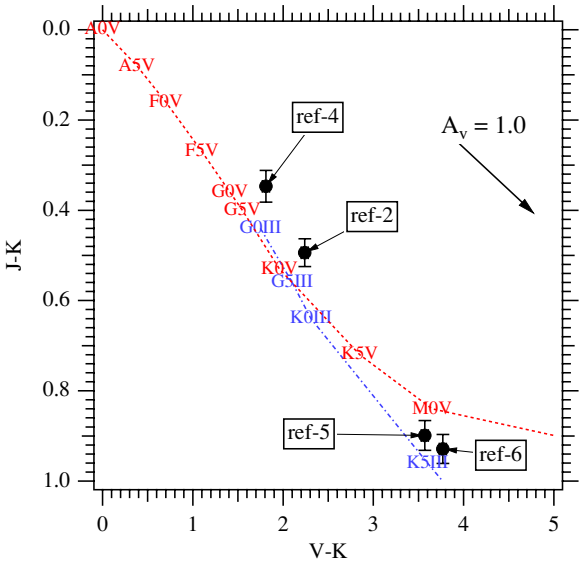

Figure 6. $(J - K)$ vs. $(V - K)$ color–color diagram for stars identified in Tables 5 and 6. The dashed line is the locus of dwarf (luminosity class V) stars of various spectral types; the dot-dashed line is for giants (luminosity class III). The reddening vector indicates $A_V = 1.0$ for the plotted color systems. Along this line-of-sight maximum extinction is $A_V \sim 2$ (Schlegel et al. 1998).

(A color version of this figure is available in the online journal.)

Table 7
Astrometric Reference Star Adopted Spectrophotometric Parallaxes

ID	Sp. T.[a]	V	M_V	$m - M$	A_V	π_{abs}(mas)
2	F2V	14.12	3	11.12	1.302	1.1 ± 0.3
4	F0V	13.05	2.7	10.35	1.147	1.4 0.3
5	K0III	13.87	0.7	13.17	1.395	0.4 0.1
6	K1III	14.34	0.6	13.74	1.271	0.3 0.1

Note. [a] Spectral types and luminosity class estimated from classification spectra, colors, and reduced proper motion diagram (Figures 6 and 7).

Micron All Sky Survey (2MASS)[10]). Table 7 lists the visible and infrared photometry for the HD 38529 reference stars. The spectra from which we estimated spectral-type and luminosity class were obtained on 2009 December 9 using the RCSPEC on the Blanco 4 m telescope at CTIO. We used the KPGL1 grating to give a dispersion of 0.95 Å pixel^{-1}. Classifications used a combination of template matching and line ratios. The spectral types for the higher S/N stars are within ±1 subclass. Classifications for the lower S/N stars are ±2 subclasses. Table 7 lists the spectral types and luminosity classes for our reference stars.

Figure 6 contains a $(J - K)$ versus $(V - K)$ color–color diagram of the reference stars. Schlegel et al. (1998) find an upper limit $A_V \sim 2$ toward HD 38529, consistent with the absorptions we infer comparing spectra and photometry (Table 7).

The derived absolute magnitudes are critically dependent on the assumed stellar luminosity, a parameter impossible to obtain for all but the latest type stars using only Figure 6. To confirm the luminosity classes obtained from classification spectra we abstract UCAC3 proper motions Zacharias et al. (2010) for a one-degree-square field centered on HD 38529, and then iteratively employ the technique of reduced proper motion (Yong & Lambert 2003; Gould & Morgan 2003) to

[10] The 2MASS is a joint project of the University of Massachusetts and the Infrared Processing and Analysis Center/California Institute of Technology.

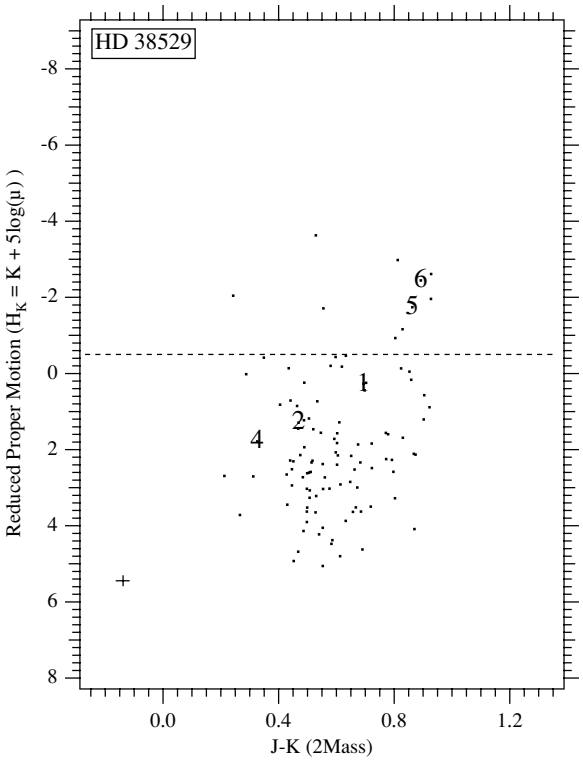

Figure 7. Reduced proper motion diagram for 107 stars in a 1/3° field centered on HD 38529. Star identifications are in Table 5. For a given spectral type, giants and sub-giants have more negative H_K values and are redder than dwarfs in $(J - K)$. H_K values are derived from proper motions in Table 9. The small cross at the lower left represents a typical $(J - K)$ error of 0.04 mag and H_K error of 0.17 mag. Ref-5 and 6 are confirmed to have luminosity class III. HD 38529 (1 in plot) is also intermediate (luminosity class IV) in this parameter space.

discriminate between giants and dwarfs. The end result of this process is contained in Figure 7. Reference stars ref-5 and ref-6 are confirmed to have luminosity class III (giant).

3.2.2. Adopted Reference Frame Absolute Parallaxes

We derive absolute parallaxes by comparing our estimated spectral types and luminosity class to M_V values from Cox (2000). Our adopted input errors for distance moduli, $(m - M)_0$, are 0.5 mag for all reference stars. Contributions to the error are uncertainties in A_V and errors in M_V due to uncertainties in color to spectral type mapping. All reference star absolute parallax estimates are listed in Table 7. Individually, no reference star absolute parallax is better determined than $\frac{\sigma_\pi}{\pi} = 23\%$. The average input absolute parallax for the reference frame is $\langle \pi_{abs} \rangle = 0.8$ mas. We compare this to the correction to absolute parallax discussed and presented in YPC95 (Section 3.2, Figure 2). Entering YPC95, Figure 2, with the Galactic latitude of HD 38529, $b = -19°$, and average magnitude for the reference frame, $\langle V_{ref} \rangle = 13.85$, we obtain a correction to absolute of 1.2 mas, consistent with our derived correction. As always (Benedict et al. 2002a, 2002b, 2002c, 2006, 2007; McArthur et al. 2004; Soderblom et al. 2005), rather than apply a model-dependent correction to absolute parallax, we introduce our spectrophotometrically estimated reference star parallaxes into our reduction model as observations with error.

3.3. The Astrometric Model

The HD 38529 reference frame contains only four stars. From positional measurements we determine the scale, rotation,

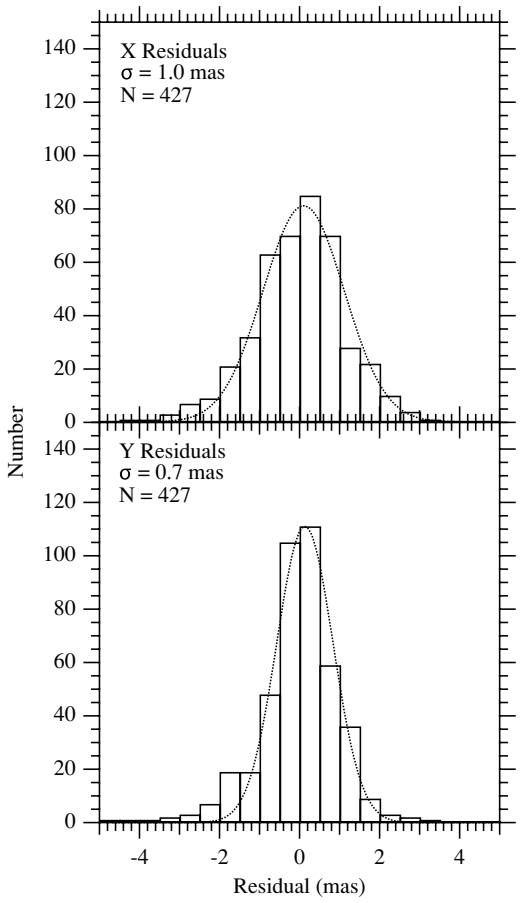

Figure 8. Histograms of x and y residuals obtained from modeling the FGS observations of HD 38529 and the FGS reference frame with Equations (4) and (5). Distributions are fit with Gaussians with standard deviations, σ, indicated in each panel.

and offset "plate constants" relative to an arbitrarily adopted constraint epoch for each observation set. As for all our previous astrometric analyses, we employ GaussFit (Jefferys et al. 1988) to minimize χ^2. The solved equations of condition for the HD 38529 field are

$$x' = x + lc_x(B-V) - XF_x \quad (2)$$

$$y' = y + lc_y(B-V) - XF_y \quad (3)$$

$$\xi = Ax' + By' + C - \mu_\alpha \Delta t - P_\alpha \pi - \mathrm{ORBIT}_x \quad (4)$$

$$\eta = Dx' + Ey' + F - \mu_\delta \Delta t - P_\delta \pi - \mathrm{ORBIT}_y \quad (5)$$

for FGS1r data. Identifying terms, x and y are the measured coordinates from *HST*; $(B-V)$ is the Johnson $(B-V)$ color of each star; and lc_x and lc_y are the lateral color corrections, applied only to FGS1r data. Here XF_x and XF_y are cross filter corrections (see Benedict et al. 2002b) in x and y applied to the observations of HD 38529. A, B, D and E are scale and rotation plate constants and C and F are offsets; μ_α and μ_δ are proper motions; Δt is the epoch difference from the constraint epoch; P_α and P_δ are parallax factors; and π is the parallax. We obtain the parallax factors from a JPL Earth orbit predictor (Standish 1990), upgraded to version DE405. Orientation to the sky for the FGS1r data is obtained from ground-based astrometry (2MASS catalog) with uncertainties of 0.°01. ORBIT_x and ORBIT_y are functions (through Thiele–Innes constants, e.g., Heintz 1978) of the traditional astrometric and RV orbital elements listed in Table 11.

Table 8
HD 38529 and Reference Star Relative Positions[a]

Star	V	ξ	σ_ξ	η	σ_η
1[b]	5.9	−2.55702	0.00013	730.32659	0.00022
2	14.1	57.28598	0.00016	661.31308	0.00016
4[c]	13.05	−14.55002	0.00011	635.50294	0.00014
5	13.87	98.23526	0.00012	647.94778	0.00014
6	14.34	−29.22806	0.00012	775.06603	0.00014

Notes.
[a] Units are arcseconds.
[b] Epoch 2005.895 (J2000); constraint plate at epoch 53965.039571, rolled to 284.°386.
[c] R.A. = 86.°642054, decl. = +1.°194295, J2000.

Table 9
Final Reference Star Proper Motions

ID	V	μ_α[a]	σ_{μ_α}	μ_δ[a]	σ_{μ_δ}
2	14.12	−13.32	0.15	15.45	0.12
4	13.05	2.32	0.09	7.87	0.09
5	13.87	−12.26	0.11	13.13	0.09
6	14.34	3.76	0.10	−4.91	0.09

Note. [a] μ_α and μ_δ are relative motions in mas yr^{-1}.

3.4. Assessing Reference Frame Residuals

The Optical Field Angle Distortion (OFAD) calibration (McArthur et al. 2002) reduces as-built *HST* telescope and FGS1r distortions with magnitude $\sim 1''$ to below 2 mas over much of the FGS1r field of regard. These data were calibrated with a revised OFAD generated by McArthur in 2007. From histograms of the FGS astrometric residuals (Figure 8) we conclude that we have obtained correction at the $\sim$1 mas level. The reference frame "catalogs" from FGS1r in ξ and η standard coordinates (Table 8) were determined with $\langle \sigma_\xi \rangle = 0.15$ and $\langle \sigma_\eta \rangle = 0.15$ mas.

3.5. The Combined Orbital Model

We linearly combine unperturbed Keplerian orbits, simultaneously modeling the RVs and astrometry. The period (P), the epoch of passage through periastron in years (T), the eccentricity (e), and the angle in the plane of the true orbit between the line of nodes and the major axis (ω), are the same for an orbit determined from RV or from astrometry. The remaining orbital elements come only from astrometry. We force a relationship between the astrometry and the RV through this constraint (Pourbaix & Jorissen 2000)

$$\frac{\alpha \sin i}{\pi_{\mathrm{abs}}} = \frac{PK(1-e^2)^{1/2}}{2\pi \times 4.7405}, \quad (6)$$

where quantities derived only from astrometry (parallax, π_{abs}, primary perturbation orbit size, α, and inclination, i) are on the left, and quantities derivable from both (the period, P and eccentricity, e), or RVs only (the RV amplitude of the primary, K), are on the right. In this case, given the fractional orbit coverage of the HD 38529c perturbation afforded by the astrometry, all right-hand side quantities are dominated by the RVs.

Table 10
Reference Frame Statistics, HD 38529 Parallax (π), and Proper Motion (μ_α, μ_δ)

Parameter	Value
Study duration	3.25 yr
Number of observation sets	23
Reference star $\langle V \rangle$	13.85
Reference star $\langle (B-V) \rangle$	1.1
HST absolute π	25.11 ± 0.19 mas
Relative μ_α	−78.69 ± 0.08 mas yr^{-1}
Relative μ_δ	−141.96 ± 0.08 mas yr^{-1}
HIP 97 absolute π	23.57 ± 0.92 mas
Absolute μ_α	−80.05 ± 0.81 mas yr^{-1}
Absolute μ_δ	−141.79 ± 0.66 mas yr^{-1}
HIP 07 absolute π	25.46 ± 0.4 mas
Absolute μ_α	−79.12 ± 0.48 mas yr^{-1}
Absolute μ_δ	−141.84 ± 0.35 masyr^{-1}

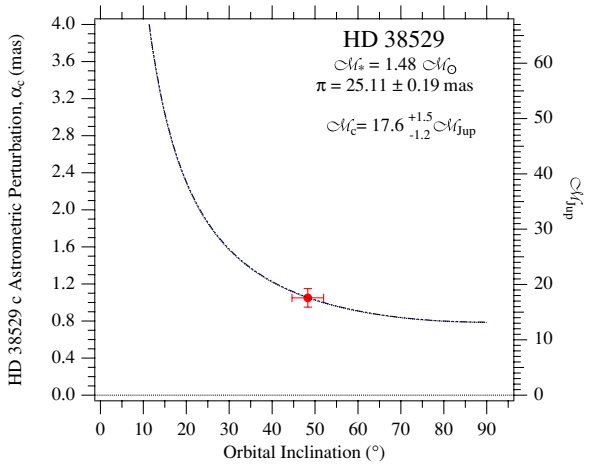

Figure 9. This curve relates perturbation size and inclination for the HD 38529c perturbation through the Pourbaix & Jorrisen (2000) relation (Equation 6). We use the curve as a "prior" in a quasi-Bayesian sense. Our final values for the semimajor axis of the astrometric perturbation, α_c, and inclination, i_c are plotted with the formal errors.

(A color version of this figure is available in the online journal.)

For the parameters critical in determining the mass of HD 38529 we find a parallax, $\pi_{abs} = 25.11 \pm 0.19$ mas and a proper motion in R.A. of -78.60 ± 0.15 mas yr^{-1} and in decl. of -141.96 ± 0.11 mas yr^{-1}. Table 10 compares values for the parallax and proper motion of HD 38529 from *HST* and both the original *Hipparcos* values and the recent *Hipparcos* re-reduction (van Leeuwen 2007). We note satisfactory agreement for parallax and proper motion. Our precision and extended study duration have significantly improved the accuracy and precision of the parallax and proper motion of HD 38529.

We find a perturbation size, $\alpha_c = 1.05 \pm 0.06$ mas, and an inclination, $i = 48.^\circ3 \pm 3.^\circ7$. These, and the other orbital elements are listed in Table 11 with 1σ errors. Figure 9 illustrates the Pourbaix & Jorrissen relation (Equation 6) between parameters obtained from astrometry (left side) and RVs (right side) and our final estimates for α_c and i. In essence, our simultaneous solution uses the Figure 9 curve as a quasi-Bayesian prior, sliding along it until the astrometric and RV residuals are minimized. Gross deviations from the curve are minimized by the high precision of all of the right-hand side terms in Equation (6) (Tables 10 and 11).

Table 11
HD38529: Orbital Parameters and Mass Including "d"

Parameter	*b*	*c*	*d*
		RV	
K (m s^{-1})	58.63 ± 0.37	170.23 ± 0.41	4.83 ± 1.3
HETγ (m s^{-1})	48.4 ± 0.6		
HJSγ (m s^{-1})	−4.7 ± 2.1		
Lick γ (m s^{-1})	−33.1 ± 0.7		
Keckγ (m s^{-1})	−85.2 ± 0.8		
		Astrometry	
α (mas)		1.05 ± 0.06	
i (°)		48.3 ± 3.7	
Ω (°)		38.2 ± 7.7	
		Astrometry and RV	
P (days)	14.3103 ± 0.0002	2136.14 ± 0.29	193.9 ± 2.9
T[a] (days)	50020.18 ± 0.08	47997.1 ± 5.9	52578.5 ± 3.3
e	0.254 ± 0.007	0.362 ± 0.002	0.23 ± 0.13
ω (°)	95.3 ± 1.7	22.1 ± 0.6	160 ± 9
		Derived[b]	
a (AU)	0.131 ± 0.0015	3.697 ± 0.042	0.75 ± 0.14
$\alpha \sin i$ (AU)	7.459e − 05 ± 3.3e − 07	3.116e − 02 ± 6.21e − 06	8.4e − 05 ± 2.4e − 05
Mass function ($M_\odot$)	2.703e − 10 ± 2.5e − 10	8.85e − 07 ± 5.0e − 9	2.1e − 12 ± 1.4e − 12
$M \sin i$ (M_J)[c]	0.90 ± 0.041	13.99 ± 0.59	0.17 ± 0.06
M (M_J)		**17.6** $^{+1.5}_{-1.2}$	

Notes.
[a] $T = T - 2400000.0$.
[b] A mass of $1.48 \pm 0.05\ M_\odot$ (Takeda et al. 2007) for HD38529 was assumed.
[c] The minimum mass.

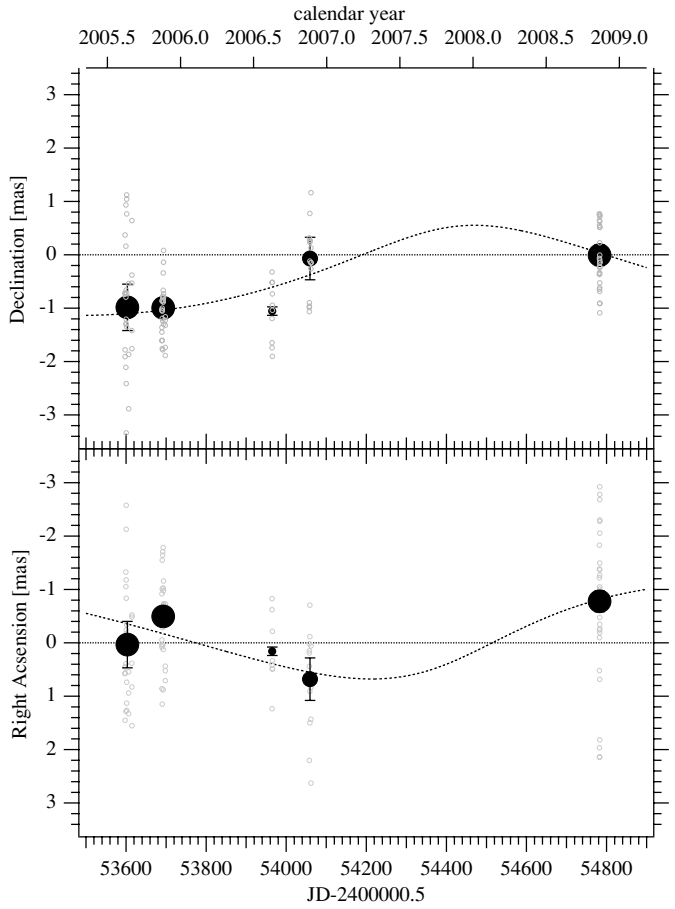

Figure 10. R.A. (bottom) and decl. (top) components of the perturbation orbit for HD 38529c as a function of time. The dashed line is the orbit described by the orbital elements found in Table 11. The small symbols are all the HD 38529 observation residuals to a model that does not contain orbital motion. The large symbols are normal points formed at each average epoch. Symbol size is proportional to the number of individual observations at each normal point epoch.

At this stage we can assess the reality of the HD 38529c astrometric perturbation by plotting the astrometric residuals from a model that does not include a component c orbit. Figure 10 shows the R.A. and decl. components of the FGS residuals plotted as small symbols. We also plot normal points formed from those smallest symbols within each of the 23 data sets listed in Table 4. The largest symbols denote the final normal points formed for each of our (effectively) five epochs. Each plot contains as a dashed line the R.A. and decl. components of the perturbation we find by including an orbit in our modeling. Finally, Figure 11 shows the perturbation on the sky with our normal points.

The planetary mass depends on the mass of the primary star, for which we have adopted $M_* = 1.48\,M_\odot$ (Takeda et al. 2007). For that M_* we find $M_c = 17.6^{+1.5}_{-1.2}\,M_{\rm Jup}$, a significant improvement over the Reffert & Quirrenbach (2006) estimate, $M_c = 38^{+36}_{-19}\,M_{\rm Jup}$, but agreeing within the errors. HD 38529c is likely a brown dwarf, but only about 3σ from the "traditional" planet–brown dwarf dividing line, 13 $M_{\rm Jup}$, the mass above which deuterium is thought to burn. In Table 11 the mass value, M_c, incorporates the present uncertainty in M_*. However, the dominant source of error is in the inclination estimate. Until HD 38529c is directly detected, its radius is unknown. Comparing to the one known transiting brown dwarf, CoRot-Exo-3b (Deleuil et al. 2008), a radius of $R \sim 1 R_{\rm JUP}$ seems reasonable.

4. LIMITS ON ADDITIONAL PLANETS IN THE HD 38529 SYSTEM

The existence of additional companions in the HD 38529 system is predicted by the "Packed Planetary Systems" hypothesis (Barnes & Raymond 2004; Raymond & Barnes 2005). Specifically those investigations identified the range of orbits in which an additional planet in between planets b and c would be stable. Having access to 11 yr of HD 38529 RV observations permits a search for longer-period companions. Our velocity database, augmented by high-cadence (Δt often less than 2 days, Table 3) HET monitoring, supports an exploration for shorter-period companions. Additionally, a relatively precise actual mass for HD 38529c better informs any companion searches based on dynamical interaction.

We independently examined the possible dynamical stability of an additional planet in the system by performing long-term *N*-body integrations of the orbits of the known planets and test particles in a manner similar to Barnes & Raymond (2004). The orbital parameters of the known planets were taken to be those we have determined. Our advantage over previous stability investigations; the true mass of planet c was used. Planet b was assumed to be coplanar with planet c, and its mass was computed based on its minimum mass and the inclination of planet c. The test particles were initialized in orbits also coplanar with planet c, and with semimajor axes ranging from 0.01 to 10.0 AU. The spacing was linear in the logarithm of the semimajor axis and 301 test particles were used. Simulations were done using three different eccentricity values for the test particles: $e = 0.0$, 0.3, and 0.7. All the calculations were carried out using the "Hybrid" integrator in the Mercury code (Chambers 1999). The simulations were performed over 10^7 yr and the integration parameters were tuned so that the fractional energy error was $<10^{-4}$.

From these simulations we find that no additional planets would be stable over long timescales interior to planet b. Between planets b and c, we find that planets with eccentricities less than 0.3 would be stable over the semimajor axis range 0.23–1.32 AU ($P = 33$–455 days). Exterior to planet c, no additional planets would be stable in orbits with periods shorter than the time baseline of the RV observations. Additional planets with eccentricities of 0.7 would not be stable over the entire range considered. These results are illustrated in Figure 12 and are completely consistent with the results of Barnes & Raymond (2004).

5. EVIDENCE FOR A POSSIBLE TERTIARY, HD 38529d

We have previously mentioned (Section 2.1) a signal in the RV data residuals that remains after the signatures of components b and c are removed. An orbital fit to those residuals from the two-component fit to HD 38529b and c is shown in the bottom panel of Figure 2 with the low-precision elements of this possible component d presented in Table 11. Table 12 contains the orbital elements from a solution in which only components b and c are modeled. While these astrometric elements closely agree with the three component solution in Table 11, the errors are larger. When HD 38529d is added to the model (adding 5 degrees of freedom, an increase of 1.5%) the χ^2 of the RV fit drops by 13%, from 287 to 258. Comparing Tables 11 and 12, we see a similar reduction in the error in the mass of component c, the

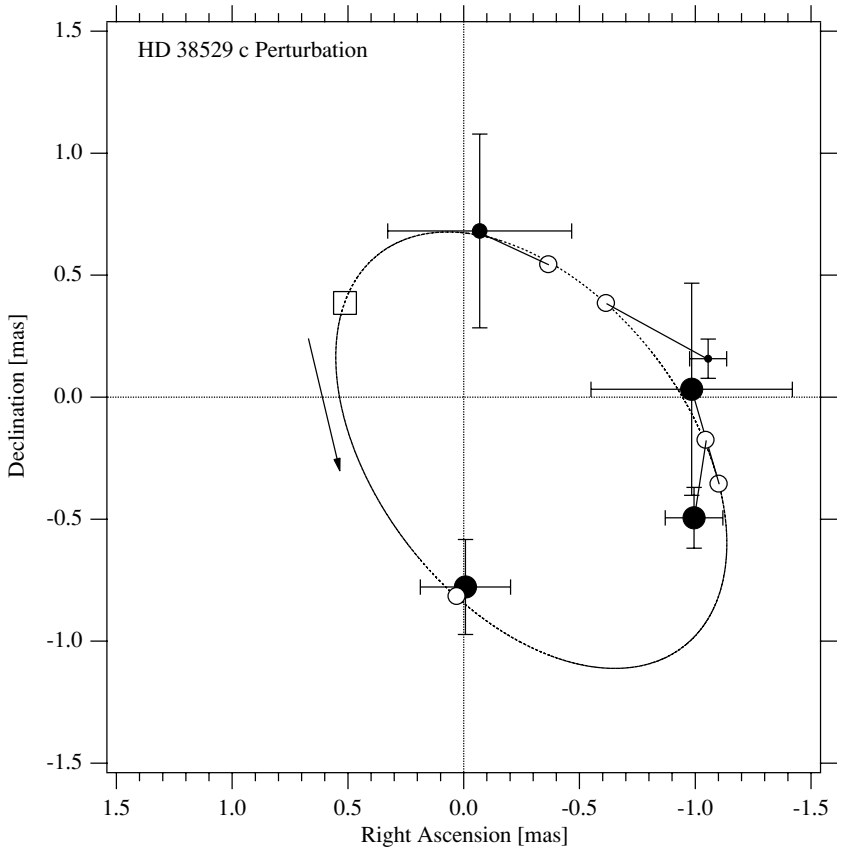

Figure 11. Perturbation orbit for HD 38529c. Elements are found in Table 11. Residual vectors are plotted, connecting each normal point residual to its predicted position (O) at each epoch of observation. Error bars indicate the positional 1σ normal point dispersion within each epoch. Normal point symbol size is proportional to the number of individual observations at each normal point epoch. The open square marks periastron passage, $T_0 = 2013.68$, and the arrow indicates the direction of perturbation motion.

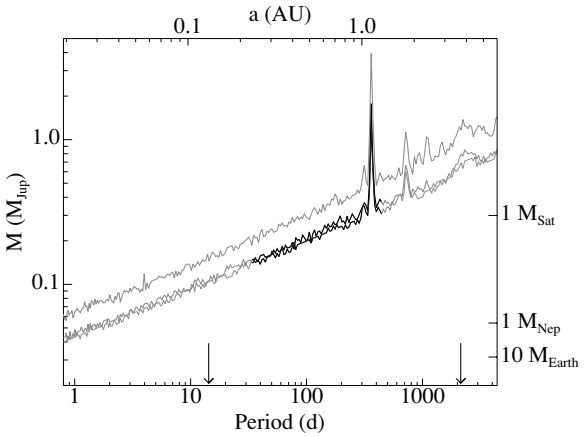

Figure 12. Results from the detection limit simulations converted to mass of a companion assuming coplanarity with HD 38529c. Values above the lines would have been detected in a periodogram analysis of the RV data. The different lines represent the different assumed eccentricity values (lower: $e = 0.0$, middle: $e = 0.3$, upper: $e = 0.7$). The black and gray parts of the lines indicate regions where test particles in the long-term simulation were stable and unstable, respectively. The arrows indicate the orbital periods of the known planets.

primary result of this study. HD 38529c remains a brown dwarf, whether or not component d is introduced.

We have explored sampling as a cause for the low-amplitude component d signal by performing power spectrum analysis of artificial RV generated from the component b and c orbits in Table 12, sampled on the dates of all the RV observations. There are no peaks at $P = 194$ days. To test for a seasonal effect in our HET data, one that might introduce a variation at the period of the tentative component d, we first removed the large-amplitude component b and c signals. We then combined the residuals containing the low amplitude signal of HD 38529d with the low amplitude signals found for HD 74156c (Bean et al. 2008) and HD 136118c (Martioli et al. 2010). The power spectrum of this aggregate should show seasonal fluctuations, if present. We saw nothing but expected signals (due to sampling) at 1/6, 1/2, and 1 yr.

Both the study in Section 4 above and the packed planetary system hypothesis Raymond et al. (2009), allow this as a potential tertiary in the system. Furthermore, a stability analysis of the system, assuming all planets lie on the same plane as planet c, demonstrated the planet is stable, consistent with the results of Barnes & Raymond (2004). We performed this test with HNBody[11] which accounts for any general relativistic precession of planet b. However, the amplitude of the HD 38529d signal is very small, $K \sim 5$ m s^{-1}, at the level of expected stellar Doppler noise (Section 2.2). The higher-cadence HET data set which could most clearly identify this object, does not span enough time for an adequate fit to the longer period HD 38529c. An unconstrained fit of HET data alone will not be possible for several more years. Therefore, we advise caution in the use of the elements listed in Table 11 and in the adoption of this signal as unequivocal evidence of a component d. Confirmation will require additional high-cadence RV observations, and/or future

[11] HNBody is publicly available at http://janus.astro.umd.edu/HNBody/.

Table 12
HD38529: Orbital Parameters and Masses for a Two-component Fit

Parameter	*b*	*c*
	RV	
K (m s^{-1})	59.17 ± 0.42	171.99 ± 0.59
HETγ (m s^{-1})	47.6 ± 0.7	
HJSγ (m s^{-1})	−4.9 ± 2.2	
Lickγ (m s^{-1})	−34.0 ± 0.8	
Keckγ (m s^{-1})	−86.9 ± 0.8	
	Astrometry	
α (mas)		1.05 ± 0.09
i (°)		48.8 ± 4.0
Ω (°)		37.8 ± 8.2
	Astrometry and RV	
P (days)	14.3104 ± 0.0002	2134.76 ± 0.40
T (days)	50020.19 ± 0.08	48002.0 ± 6.2
e	0.248 ± 0.007	0.360 ± 0.003
ω (°)	95.9 ± 1.7	22.52 ± 0.7
	Derived	
a (AU)	0.131 ± 0.0015	3.695 ± 0.043
$\alpha \sin i$ (AU)	7.540e − 05 ± 3.9e − 07	3.149e − 02 ± 7.37e − 06
Mass function ($M_\odot$)	2.792e − 10 ± 4.4e − 10	9.137e − 07 ± 6.1e − 9
$M \sin i$ (M_J)	0.92 ± 0.043	14.13 ± 0.62
M (M_J)		**17.7** $^{+1.7}_{-1.4}$

astrometry. A minimum mass component d would generate a peak-to-peak astrometric signature of 52 microseconds of arc, likely detectable by Gaia (Casertano et al. 2008).

6. DISCUSSION AND CONCLUSIONS

6.1. Discussion

Given the adopted Table 11 errors, HD 38529c is either one of the most massive exoplanets or one of the least massive brown dwarfs. We can compare our true mass to the (as of 2010 January) 69 transiting exoplanetary systems, each also characterized by true mass, not $M \sin i$. As shown in the useful Exoplanetary Encyclopedia (Schneider 2009) only one companion (CoRoT-Exo-3 b, Deleuil et al. 2008) has a mass in excess of 13 $M_{\rm Jup}$. Whether this "brown dwarf desert" (Grether & Lineweaver 2006) in the transiting sample is due to the difficulty of migrating high-mass companions (bringing them in close enough to increase the probability of transit), or to inefficiencies in gravitational instability formation is unknown.

The age of the host star, ∼3.3 By, would suggest that HD 38529c has not yet cooled to an equilibrium temperature. An estimated temperature and self-luminosity for a 17 $M_{\rm Jup}$ object that is 3.3 By old can be found from the models of Hubbard et al. (2002). Those models predict that HD 38529c has an effective temperature, $T_{\rm eff} \simeq 400$ K, and $L = 2.5e{-}7\ L_\odot$, about 20 times brighter than what we estimated using these same models for ϵ Eri b (Benedict et al. 2006). Unfortunately HD 38529 has about 16 times the intrinsic brightness of ϵ Eri, erasing any gain in contrast. We note that due to the eccentricity of the orbit, HD 38529c is actually within the present-day habitable zone for a fraction of its orbit. As HD 38529 continues to evolve and brighten, the habitable zone will move outward and HD 38529c will be in that zone for some period of time.

If the inner known companion HD 38529b is a minimum mass exoplanetary object (assuming $M = M \sin i = 0.8\ M_{\rm Jup}$), our 1 mas astrometric per-observation precision precludes detecting that 2 mas of arc signal. Invoking (with no good reason) coplanarity with HD 38529c similarly leaves us unable to detect HD 38529b. However, with the motivation of our previous result for HD 33636 (Bean et al. 2007), we can test whether or not HD 38529b is also stellar by establishing an upper limit from our astrometry. To produce a perturbation, $\alpha_b > 0.2$ mas (a 3σ detection, given $\sigma_\alpha = 0.06$ mas from Table 11), and the observed RV amplitude, $K_b = 59$ m s^{-1}, requires $M_b \sim 0.1\ M_\odot$ in an orbit inclined by less than 0.°5. Our limit is lower than that established with the CHARA interferometer (Baines et al. 2008a), who established a photometric upper limit of G5 V for the b component. While it might be possible to use 2MASS and SDSS (Ofek 2008) photometry of this object to either confirm or eliminate a low-mass stellar companion by backing out a possible contribution from an M, L, or T dwarf, using their known photometric signatures (Hawley et al. 2002; Covey et al. 2007), we lack precise (1%) knowledge of the intrinsic photometric properties of a sub-giant star in the Hertzsprung gap with which to compare.

6.2. Conclusions

In summary, RVs from four sources, Lick and Keck (Wright et al. 2009), HJS/McDonald (Wittenmyer et al. 2009), and our new high-cadence series from the HET, were combined with *HST* astrometry to provide improved orbital parameters for HD 38529b and HD 38529c. Rotational modulation of star spots with a period $P = 31.66 \pm 0.17$ days produces 0.15% photometric variations, spot coverage sufficient to produce the observed residual RV variations. Our simultaneous modeling of RVs and over three years of *HST* FGS astrometry yields the signature of a perturbation due to the outermost known companion, HD 38529c. Applying the Pourbaix & Jorrissen constraint between astrometry and RVs, we obtain for the perturbing object HD 38529c a period, $P = 2136.1 \pm 0.3$ days, inclination, $i = 48.°3 \pm 3.°7$, and perturbation semimajor axis, $\alpha_c = 1.05 \pm 0.06$ mas. Assuming for HD 38529a stellar mass

$M_* = 1.48 \pm 0.05\,M_\odot$, we obtain a mass for HD 38529c, $M_b = 17.6^{+1.5}_{-1.2}\ M_{\rm Jup}$, within the brown dwarf domain. Our independently determined parallax agrees within the errors with *Hipparcos*, and we find a close match in proper motion. Our HET RVs combined with others establish an upper limit of about one Saturn mass for possible companions in a dynamically stable range of companion-star separations, $0.2 \leqslant a \leqslant 1.2$ AU. RV residuals to a model incorporating components b and c contain a signal with an amplitude equal to the rms variation with a period, $P \sim 194$ days and an inferred $a \sim 0.75$ AU. While dynamical simulations do not rule out interpretation as a planetary mass companion, the low S/N of the signal argues for confirmation.

We thank the Carnegie–California Exoplanet Consortium, particularly J. T. Wright, for access to their improved HD 38529 velocities in advance of publication. Support for this work was provided by NASA through grants GO-10610, GO-10989, and GO-11210 from the Space Telescope Science Institute, which is operated by the Association of Universities for Research in Astronomy, Inc., under NASA contract NAS5-26555. J.L.B. acknowledges support from the DFG through grants GRK 1351 and RE 1664/4-1, and the European Commission's Seventh Framework Programme as an International Fellow (grant no. PIFF-GA-2009-234866). The HET is a joint project of the University of Texas at Austin, the Pennsylvania State University, Stanford University, Ludwig-Maximilians-Universität München, and Georg-August-Universität Göttingen. The HET is named in honor of its principal benefactors, William P. Hobby and Robert E. Eberly. We thank the many Resident Astronomers and Telescope Operators whose efforts produced the high-quality spectra from which our HET velocities were extracted. T.H. was a Visiting Astronomer, Cerro Tololo Inter-American Observatory, National Optical Astronomy Observatory, which is operated by the Association of Universities for Research in Astronomy, Inc., under cooperative agreement with the National Science Foundation. This publication makes use of data products from the 2MASS, which is a joint project of the University of Massachusetts and the Infrared Processing and Analysis Center/California Institute of Technology, funded by NASA and the NSF. This research has made use of the SIMBAD database, operated at Centre Données Stellaires, Strasbourg, France; Aladin, developed and maintained at CDS; the NASA/IPAC Extragalactic Database (NED) which is operated by JPL, California Institute of Technology, under contract with NASA; the Exoplanet Encyclopedia (grace á J. Schneider); and NASA's Astrophysics Data System Abstract Service. An anonymous referee motivated improvements to the clarity of presentation for which we are thankful.

REFERENCES

Baines, E. K., et al. 2008a, ApJ, 682, 577
Baines, E. K., et al. 2008b, ApJ, 680, 728
Barnes, R., & Raymond, S. N. 2004, ApJ, 617, 569
Bean, J. L., et al. 2007, AJ, 134, 749
Bean, J. L., et al. 2008, ApJ, 672, 1202
Benedict, G. F., et al. 1998, AJ, 116, 429
Benedict, G. F., et al. 2002a, ApJ, 581, L115
Benedict, G. F., et al. 2002b, AJ, 124, 1695
Benedict, G. F., et al. 2002c, AJ, 123, 473
Benedict, G. F., et al. 2006, AJ, 132, 2206
Benedict, G. F., et al. 2007, AJ, 133, 1810
Casertano, S., et al. 2008, A&A, 482, 699
Chambers, J. E. 1999, MNRAS, 304, 793
Cochran, W. D., et al. 2004, ApJ, 611, L133
Covey, K. R., et al. 2007, AJ, 134, 2398
Cox (ed.), A. N. 2000, Allen's Astrophysical Quantities, 4th ed. (New York: AIP)
Deleuil, M., et al. 2008, A&A, 491, 889
Fischer, D. A., et al. 2001, ApJ, 551, 1107
Fischer, D. A., et al. 2003, ApJ, 586, 1394
Gould, A., & Morgan, C. W. 2003, ApJ, 585, 1056
Grether, D., & Lineweaver, C. H. 2006, ApJ, 640, 1051
Hatzes, A. P. 2002, Astron. Nachr., 323, 392
Hatzes, A. P., & Zechmeister, M. 2008, J. Phys. Conf. Ser., 118, 012016
Hatzes, A. P., et al. 2005, A&A, 437, 743
Hawley, S. L., et al. 2002, AJ, 123, 3409
Heintz, W. D. 1978, Double Stars (Dordrecht: Reidel)
Hubbard, W. B., Burrows, A., & Lunine, J. I. 2002, ARA&A, 40, 103
Jefferys, W. H., Fitzpatrick, M. J., & McArthur, B. E. 1988, Celest. Mech., 41, 39
Kjeldsen, H., & Bedding, T. R. 1995, A&A, 293, 87
Martioli, E., et al. 2010, ApJ, 708, 625
McArthur, B., et al. 2002, in The 2002 HST Calibration Workshop: Hubble after the Installation of the ACS and the NICMOS Cooling System, ed. S. Arribas, A. Koekemoer, & B. Whitmore (Baltimore, MD: STScI), 373
McArthur, B. E., et al. 2004, ApJ, 614, L81
Moro-Martín, A., et al. 2007, ApJ, 668, 1165
Murray, N., & Chaboyer, B. 2002, ApJ, 566, 442
Nelan, E. P. 2007, Fine Guidance Sensor Instrument Handbook (16th ed.; Baltimore, MD: STScI)
Ofek, E. O. 2008, PASP, 120, 1128
Pourbaix, D., & Jorissen, A. 2000, A&AS, 145, 161
Raymond, S. N., & Barnes, R. 2005, ApJ, 619, 549
Raymond, S. N., et al. 2009, ApJ, 696, L98
Reffert, S., & Quirrenbach, A. 2006, A&A, 449, 699
Saar, S. H., & Donahue, R. A. 1997, ApJ, 485, 319
Schlegel, D. J., Finkbeiner, D. P., & Davis, M. 1998, ApJ, 500, 525
Schneider, J. 2009, Extrasolar Planets Encyclopedia (http://exoplanet.eu/index.php)
Soderblom, D. R., et al. 2005, AJ, 129, 1616
Standish, E. M., Jr. 1990, A&A, 233, 252
Takeda, G., et al. 2007, ApJS, 168, 297
Takeda, Y. 2007, PASJ, 59, 335
Tull, R. G. 1998, Proc. SPIE, 3355, 387
Valenti, J. A., & Fischer, D. A. 2005, ApJS, 159, 141
van Altena, W. F., Lee, J. T., & Hoffleit, E. D. 1995, The General Catalogue of Trigonometric [Stellar] Parallaxes (4th ed.; New Haven, CT: Yale Univ. Observatory)
van Leeuwen, F. 2007, in Astrophysics and Space Science Library 350, Hipparcos, the New Reduction of the Raw Data (Dordrecht: Springer)
van Leeuwen, F., et al. 2007, MNRAS, 379, 723
Wittenmyer, R. A., et al. 2009, ApJS, 182, 97
Wright, J. T., et al. 2009, ApJ, 693, 1084
Yong, D., & Lambert, D. L. 2003, PASP, 115, 796
Zacharias, N., et al. 2010, AJ, in press (arXiv:1003.2136)